



Universidad Autónoma
de Madrid

Biblos-e Archivo
Repositorio Institucional UAM

Repositorio Institucional de la Universidad Autónoma de Madrid
<https://repositorio.uam.es>

Esta es la **versión de autor** del artículo publicado en:
This is an **author produced version** of a paper published in:

Journal of Food Engineering 222 (2018): 199-206

DOI: <https://doi.org/10.1016/j.jfoodeng.2017.11.027>

Copyright: © 2017 Elsevier Ltd.

El acceso a la versión del editor puede requerir la suscripción del recurso
Access to the published version may require subscription

Supercritical extraction of solid materials: a practical correlation related with process scaling

Alexis López-Padilla, Alejandro Ruiz-Rodriguez*, Guillermo Reglero and Tiziana Fornari

Institute of Food Science Research CIAL (CSIC-UAM) – CEI UAM + CSIC,

Madrid, 28049, Spain

* Correspondence: alejandro.ruiz@uam.es; Tel.: +34 -910-017-923

15 **Abstract**

16 The supercritical fluid extraction (SFE) of vegetal raw materials is a large field of research,
17 innovation and entrepreneurial developments. Optimization of process conditions is usually
18 accomplished in analytical or laboratory scale equipment. Although SFE scaling is essential to
19 attain industrial applications, studies in the literature are scarce. In this work, the kinetic
20 behavior of 19 overall extraction curves (OEC's), obtained by the authors in previous works
21 using NOVALINDUS Platform SFE facilities, and a set of 39 OEC's published by other authors,
22 were considered all together to study SFE scaling. A general trend between the solvent flow
23 rate and Barton kinetic constant was obtained for all extraction curves included in the data
24 base, which comprise 10 different plant materials, temperatures in the range 298-333 K,
25 pressures of 10-30 MPa, extractor volumes from 50 to 5200 cm³, particle diameters from
26 250 to 1400 µm and bed porosity in the range 0.59-0.97.

27

28

29 **Keywords:** *Supercritical fluid extraction; Overall extraction curve; Mass transfer; Barton*
30 *model; Scaling up.*

31

32

33 1. Introduction

34 The kinetic behavior of the Supercritical Fluid Extraction (SFE) of solid materials is usually
35 represented by the plot of the mass extracted as a function of time or as a function of the
36 mass of spent solvent. This representation is commonly called the Overall Extraction Curve
37 (OEC). Not only mass yield varies along extraction time, but also composition,
38 physicochemical and biological properties of the extract (García-Risco et al., 2011a; Zabot et
39 al., 2014a). SFE scaling aims to reproduce the same kinetic behavior in extraction vessels
40 with different shape and/or capacity.

41 A large number of kinetic models can be found in the literature, which were developed to
42 represent the OEC of SFE processes, including simple correlations based on first order
43 kinetics, such as the Barton model (Cháfer and Berna, 2014; Nguyen et al., 1991; Silva et al.,
44 2011, 2008), to comprehensive phenomenological models based on mass transfer
45 differential made in the cell extraction (De Melo et al., 2014; Huang et al., 2012; Oliveira et
46 al., 2011). Yet, more limited approaches and studies are available in the literature regarding
47 SFE scaling. Studies are mainly based on some thumb rules or semi-empirical approaches
48 based on traditional chemical engineering fundamentals and adapted for high pressure SFE
49 process. For example, keeping constant the ratio between solvent flow rate and biomass
50 weight, or keeping constant the ratio between the mass weight of solvent spent and of
51 biomass weight (Prado et al., 2012, 2011; Yesil-Celiktas et al., 2009), maintaining constant
52 the solvent linear velocity, or the solvent residence time, among others, are very common
53 scaling criteria applied in SFE (López-Padilla et al., 2016b).

54 SFE vessels are in general cylindrical. Vessel length and internal diameter are usually used to
55 describe bed geometry, which also affect significantly the extraction. Furthermore, the ratio

56 between height and diameter of the packed bed has been used to validate some scaling
57 approaches (Prado et al., 2012).

58 For example, Carvalho et al. (2005) and Zabet et al. (2014a, 2014b) found good scaling
59 results in the SFE of rosemary and clove buds by applying the solvent to feed mass ratio
60 criterion combined with maintaining the height/diameter ratio. Paula et al. (2016) evaluated
61 the effect of bed geometry using the criterions of constant residence time or constant CO₂
62 velocity in the scaling up SFE process for *Baccharis dracunculifolia* and found that the second
63 one was appropriate. Recently, López-Padilla et al. (2017) studied the SFE scaling of
64 *Calendula officinalis* and the experiments proved that constant CO₂ residence time was an
65 adequate scaling criterion for a scaling factor around 5, while the constant CO₂ velocity was
66 the criterion suitable for a larger scaling factor close to 20.

67 Thus, in general, there is not a single criterion effective for SFE scaling and more studies are
68 required to get more information about the influence of the large set of variables that can
69 affect the extraction kinetics. In this respect, López-Padilla et al. (2017) has recently
70 correlated the mass transfer coefficients (Broken and Intact Cell model) of calendula OECs
71 obtained in cells of diverse size, at different extraction pressures and temperatures, in terms
72 of the CO₂ flow rate, the extraction cell geometric parameters (diameter and length) and the
73 dimensionless Schmidt number. The correlation was derived keeping constant bed porosity
74 and mean particle size of calendula raw material.

75 In this work, this correlation was extended to consider a variety of plant raw materials of
76 different apparent density, porosity and particle size. First, a set of 19 OECs obtained by the
77 authors in previous works using their SFE facilities (NOVALINDUS Platform) were considered,
78 and then the correlation developed was tested using a set of 34 OECs reported by other
79 authors in the literature.

80 **2. Fundamentals and data base**

81 In the SFE of solid raw materials, the mass extracted and thus the extraction yield (mass
82 extracted / mass loaded in the extraction vessel) increases with time, defining the typical
83 shape of the overall extraction curve (OEC) (see Figure 1). The rate of solutes mass transfer
84 from the surface of the solid particles to the core of the supercritical solvent depends
85 significantly on the mass transfer coefficient and the interfacial area. The objective of this
86 work is to investigate the relation between these process variables and the solvent flow rate,
87 considering a large set of OEC data, related with the SFE of different plant materials, and
88 taking into account the variability of process conditions (temperature and pressure),
89 extraction cell dimensions (diameter and height) and packed bed characteristics (apparent
90 density, porosity).

91 The mass transfer coefficient of a specific OEC can be estimated using a variety of kinetic
92 models. Although accurate and theoretical-based models are available in the literature,
93 these models usually demand several fitting parameters besides the mass transfer
94 coefficient, and require specific software and mathematical routines for the fitting
95 procedure. On the other side, Nguyen et al. (1991) presented a single model to express the
96 mass rate out of a solid matrix, by describing the solutes extraction as a first-order-type
97 reaction. Because of its simplicity, Barton model was used in this work to estimate the mass
98 transfer coefficient of all OEC data compiled from the literature, as described in the
99 following section.

100

101 **2.1 Barton model**

102 The overall extraction curve (OEC) according to Barton model can be described as a first-
103 order-type reaction:

$$Y = Y_{\infty}[1 - \exp(-kt)] \quad (1)$$

Where Y is the extraction yield (mass extracted / mass loaded in the extraction vessel), Y_{∞} is the extraction yield when $t \rightarrow \infty$ and k is Barton kinetic constant. The accumulated mass of extract versus time (Y vs. t) of a OEC can be represented using Eq. (1) by the linear regression of $\ln(1 - Y/Y_{\infty})$ vs. t , and considering the simultaneous fitting of parameters k and Y_{∞} to minimize the corresponding regression coefficient (R^2).

2.2 Kinetic data compiled

2.2.1 OECs from NOVALINDUS Platform

NOVALINDUS is a technological platform comprising SFE facilities of diverse capacities which were used by the authors in previous works (Fornari et al., 2012; García-Risco et al., 2011b; López-Padilla et al., 2016b; Villanueva-Bermejo et al., 2017) to extract a variety of vegetal materials. Table 1 reports the characteristics of the facilities and extractor vessels available in NOVALINDUS Platform.

The extraction conditions of different SFE experiments are given in Table 2 and comprise 19 OECs concerning the extraction of seven different plants: oregano, sage, thyme, rosemary, yarrow, calendula and mortiño. For each OEC, Table 2 reports the diameter (D) and length (L) of the corresponding cylindrical extraction vessel, the characteristics of the packed bed (type of plant, mass loaded F , particle diameter d_p , plant density ρ_B and bed porosity ε) and the SFE extraction conditions (temperature T , pressure P and CO_2 flow rate Q).

CO_2 density ρ_{CO_2} and viscosity μ_{CO_2} were calculated using an equation of state proposed by Span and Wagner (Tegeler et al., 1999) and involved in an open web source by NIST Webbook (NIST, 2017). This equation resulted from an empirical representation of the fundamental equation based on Helmholtz energy in dependence on density and

128 temperature. This equation shows lower relative deviations between experimental and
129 predicted values $\pm 0.2\%$ under supercritical pressures and temperatures extraction
130 processes. CO_2 viscosity μ_{CO_2} was calculated as a function of temperature and pressure,
131 using a correlation specifically derived for carbon dioxide (Fenghour et al., 1998) and linked
132 by the NIST Webbook.

133 The diffusion coefficient of the extract in CO_2 ($D_{E-\text{CO}_2}$) was estimated using the equation
134 recently given by López-Padilla et al. (2016a) for plant essential oils in supercritical CO_2 :

$$135 \quad D_{E-\text{CO}_2} = 3.5400 \times 10^{-4} + 1.1129 \times 10^{-3} \mu_{\text{CO}_2} - 4.3036 \times 10^{-4} \rho_{\text{CO}_2} + 1.64 \times 10^{-7} T \quad (2)$$

136 Where $D_{E-\text{CO}_2}$ is given in $\text{cm}^2 \cdot \text{s}^{-1}$, μ_{CO_2} is given in cP, ρ_{CO_2} in $\text{g} \cdot \text{cm}^{-3}$ and T in $^\circ\text{C}$. It is assumed
137 that Eq. (2) provides a satisfactory estimation of the diffusion coefficient of all extracts
138 obtained in the OECs from NOVALINDUS Platform.

139 The Schmidt dimensionless number was calculated according to:

$$140 \quad S_c = \frac{\mu_{\text{CO}_2}}{\rho_{\text{CO}_2} D_{E-\text{CO}_2}} \quad (3)$$

141 Where $D_{E-\text{CO}_2}$ is given in $\text{m}^2 \cdot \text{s}^{-1}$, μ_{CO_2} is given in $\text{kg} \cdot \text{m}^{-1} \cdot \text{s}^{-1}$ and ρ_{CO_2} in $\text{kg} \cdot \text{m}^{-3}$. The values
142 obtained are given in Table 2.

143 **2.2.2 OECs from the literature**

144 Similarly to Table 2, Table 3 gives the data corresponding to 34 OECs reported by different
145 authors concerning the SFE of red pepper (Silva and Martínez, 2014), chamomile (Povh et al.,
146 2001) and ginger (Martinez et al., 2003; Zancan et al., 2002). CO_2 density (ρ_{CO_2}) and
147 viscosity (μ_{CO_2}), the diffusion coefficient ($D_{E-\text{CO}_2}$) and Schmidt number (S_c) were
148 calculated as described in previous section, except the diffusion coefficient of red pepper
149 extracts (Silva and Martínez, 2014) in which case the diffusion coefficient was calculated

150 according to the correlation of López-Padilla et al. (2016a) for plant fixed oils in supercritical
151 CO₂:

$$152 \quad D_{E-CO_2} = 8.5244 \times 10^{-5} + 1.4097 \times 10^{-4} \mu_{CO_2} - 8.0482 \times 10^{-5} \rho_{CO_2} + 1.96 \times 10^{-7} T \quad (4)$$

153 Bed porosity (ε) is according the value reported in the corresponding literature source, but
154 the value was checked to satisfy the following equation:

$$155 \quad \varepsilon = 1 - \frac{\rho_{app}}{\rho_B} = 1 - \frac{4F}{\pi D^2 L \rho_B} \quad (5)$$

156 Where ρ_{app} is the apparent density of the packed bed.

157

158 **3. Results and Discussion**

159 **3.1 Correlation of Barton kinetic constants of calendula OECs obtained in NOVALINDUS** 160 **Platform**

161 In previous work, the scaling of calendula SFE was studied (López-Padilla et al., 2017). Nine
162 OECs were obtained using the extraction cells of different size available in NOVALINDUS
163 Platform (Table 1) and were represented using the Broken and Intact Cell (BIC) model
164 (Sovová, 2017; Sovová, 1994). With the purpose of developing a scaling correlation
165 applicable among NOVALINDUS facilities, the regressed BIC mass transfer coefficients in the
166 supercritical fluid phase (k_{YA}) were correlated with the CO₂ flow rate (Q). The scaling
167 correlation (see Figure 2) includes the extractor diameter and length, and the dimensionless
168 Schmidt number (S_c). Bed porosity and particle size were not included in the correlation
169 because these parameters were kept constant during calendula SFE.

170 In this work, the same nine calendula OECs of previous work (López-Padilla et al., 2017) were
171 represented using Barton model (Eq. 1), and the type of relation depicted in Figure 2 was
172 tested using Barton kinetic constant (k) instead of BIC mass transfer coefficient (k_{YA}).

173 Tables 4 gives the values obtained for k , together with the Y_{∞} value which minimize the
174 regression coefficient (R^2), which is also given in the table. In general, Barton k values were
175 one order of magnitude lower than BIC k_{YA} values (López-Padilla et al., 2017). As sake of
176 comparison, Figure 3 show BIC and Barton model representations for two selected calendula
177 OECs. Figure 3(a) correspond to OEC 11 in Table 2, for which BIC model resulted better than
178 Barton model, while the opposite resulted in the case of Figure 3(b) corresponding to OEC 17
179 in Table 2 (worse R^2 value of Barton model fitting).

180 Figure 4 shows the same relation depicted in Figure 2 using the regressed Barton k values. It
181 can be clearly stated from the figure that the correlation reported in previous work (Figure
182 2) is still valid and effective in the case of using Barton kinetic constants instead of BIC mass
183 transfer coefficients. The regression coefficient obtained in Figure 4 is $R^2 = 0.9906$, slightly
184 higher than the one obtained in Figure 2 ($R^2 = 0.9767$).

185 **3.2 Extension of the correlation to other OECs obtained in NOVALINDUS Platform**

186 As mentioned in previous section, the correlation presented in Figures 2 and 4 do not
187 include bed porosity or mean particle diameter of plant material, because all calendula OECs
188 were carried out keeping constant these two variables.

189 With the objective of analyze the influence of ε and d_p in the SFE scaling correlation, the 19
190 OECs obtained in the three different scale supercritical plants available in NOVALINDUS
191 Platform (Table 2) were considered all together. These OECs include extractions with bed
192 porosity in the range of 0.59 - 0.82 and particle diameter in the range of 250 - 1000 μm .

193 It was observed that the inclusion of the specific interfacial area (a_0) defined by:

$$194 \quad a_0 = 6(1 - \varepsilon)/d_p \quad (6)$$

195 Resulted in a good correlation of all OEC Barton k values regressed (which are reported in
196 Table 3) with $R^2 = 0.9647$. Then, CO_2 density was also included with the aim of attain a

197 dimensionless relation between the abscissa and ordinate of the correlation. Figure 5(a)
198 shows the final result, with a regression coefficient $R^2 = 0.9594$, very similar to the
199 previous one. Then, the correlation depicted in Figure 5(a) provides a fundamental relation
200 between the main variables affecting the kinetic behavior of the SFE extractions carried out
201 in NOVALINDUS Platform (Table 2) and can be a useful tool for SFE scaling.

202 3.3 Applying the scaling correlation to OECs from the literature

203 The correlation developed considering the OEC data produced by the authors in
204 NOVALINDUS Platform was tested using the OEC data from the literature given in Table 3. A
205 total of 34 OECs were compiled. Although a larger number was originally considered, many
206 were discarded due to the lack of information, mainly bed porosity, extraction cell
207 dimensions, plant material density, or the kinetic data was insufficient and/or do not allow
208 an accurate estimation of Y_{∞} .

209 In order to fit the Barton kinetic constant for each OEC, in several cases and due to the
210 absence of numerical data, the experimental OECs (Y vs t points) were taken from the plots
211 available in the corresponding published works, using the open software Plot Digitizer v.
212 2.6.6 (Huwaldt and Steinhorst, 2014). The Barton k values regressed, together with the Y_{∞}
213 and R^2 values obtained are given in Table 4.

214 Figure 5(b) shows the correlation between the Barton k values and solvent flow rate for the
215 19 NOVALINDUS OECs plus the 34 OECs from the literature. Despite the regression
216 coefficient obtained is somewhat smaller $R^2 = 0.8328$ the general trend of the scaling
217 correlation proposed in this work is confirmed.

218 On the other hand, the mass transfer coefficient is commonly correlated in the literature as
219 a function of the dimensionless Schmidt (Sc) and Reynolds (Re) numbers. The Sc number
220 was exposed as an important parameter in the correlations developed, as can be observed in

221 Figures 4 and 5. However, the effect of *Re* number is hidden in the analysis presented in this
222 work.

223 Reynold dimensionless number, defined as:

$$224 \quad Re = \frac{\rho_{CO_2} U d_p}{\mu_{CO_2}} \quad (7)$$

225 Where *U* is the CO₂ velocity and *d_p* is the mean particle diameter of the raw material.

226 *Re* number was calculated for all OECs of Tables 2 and 3, and its effect on the correlation
227 was studied. For this purpose, linear regressions were carried out taking into account
228 separately data with high or small *Re* numbers. The results of this analysis is depicted in
229 Figure 6, where it can be observed that the linear regression of data with *Re* numbers in the
230 range 7.37-17.43 (Figure 6a) provides a slope 2.3 times higher than in the case of data with
231 considerably lower *Re* numbers (0.16-0.34) (Figure 6b). Furthermore, higher regression
232 coefficients were obtained in both cases, in comparison with the regression coefficient
233 obtained considering the data all together. This means that the *Re* number of the OEC
234 strongly affects the slope of the linear regression. Much more experimental OEC data,
235 including other raw materials, process conditions and extractor dimensions, is being
236 compiled in order to trustworthy elucidate this effect and to guarantee the accuracy of the
237 developed scaling up procedure.

238

239 **Conclusions**

240 The relation between the solvent flow rate (*Q*) in plant material SFE and the mass transfer
241 coefficient was studied. A large set of OECs was compiled from the literature, including 19
242 OECs obtained by the authors in NOVALINDUS Platform and 34 OECs from the literature.
243 OEC data comprise 10 different plant materials, temperatures in the range 298-333 K and
244 pressures in the range 10-30 MPa. Additionally, particle diameter varied from 250 to 1400

245 μm , extractor volume from 50 to 5200 cm^3 and bed porosity was in the range 0.59-0.97. All
246 OECs were correlated using Barton model, by fitting the Barton kinetic constant k and
247 achieving regression coefficients higher than 0.90.

248 A relation between the solvent flow rate and Barton kinetic constant observed in previous
249 work (López-Padilla et al., 2017), which was developed for a single plant material and an
250 unique particle diameter and bed porosity, was reasonably extended to cover the wider
251 extraction conditions and materials covered in the 53 OECs compiled in this work, and
252 demonstrated a general trend which can be used for estimating the solvent flow rate
253 required in SFE scaling. Furthermore, it was observed that the slope of the correlation is
254 highly affected by Reynolds number. Studies are in progress, extending the data set of OECs,
255 to elucidate this effect in the scaling procedure.

256

257 **Acknowledges**

258 López-Padilla A. Thanks to COLCIENCIAS (568–2012) and Medellin Mayor's Office
259 (Sapiencia/Enlaza Mundos Program, 2013) for the Ph.D. fellowship. This work was financed
260 thanks ALIBIRD, S2013/ABI-2728 (Comunidad de Madrid) project.

261

262

263 References

264

265 Carvalho, R.N., Moura, L.S., Rosa, P.T. V, Meireles, M.A.A., 2005. Supercritical fluid extraction
266 from rosemary (*Rosmarinus officinalis*): Kinetic data, extract's global yield,
267 composition, and antioxidant activity. Journal of Supercritical Fluids 35, 197–204.
268 <https://doi.org/10.1016/j.supflu.2005.01.009>.

269 Cháfer, A., Berna, A., 2014. Study of kinetics of the d-pinitol extraction from carob pods using
270 supercritical CO₂. Journal of Supercritical Fluids 94, 212–215.
271 <https://doi.org/10.1016/j.supflu.2014.07.015>.

272 De Melo, M.M.R., Silvestre, A.J.D., Silva, C.M., 2014. Supercritical fluid extraction of
273 vegetable matrices: Applications, trends and future perspectives of a convincing green
274 technology. The Journal of Supercritical Fluids 92, 115–176.
275 <https://doi.org/10.1016/j.supflu.2014.04.007>.

276 Fenghour, A., Wakenham, W.A., Vesovic, V., 1998. The Viscosity of Carbon Dioxide. Journal
277 of Physical and Chemical Reference Data 27, 31–44. doi:10.1098/rspa.1912.0058

278 Fornari, T., Ruiz-Rodriguez, A., Vicente, G., Vázquez, E., García-Risco, M.R., Reglero, G., 2012.
279 Kinetic study of the supercritical CO₂ extraction of different plants from Lamiaceae
280 family. The Journal of Supercritical Fluids 64, 1–8.
281 <https://doi.org/10.1016/j.supflu.2012.01.006>.

282 García-Risco, M.R., Hernández, E.J., Vicente, G., Fornari, T., Señoráns, F.J., Reglero, G., 2011a.
283 Kinetic study of pilot-scale supercritical CO₂ extraction of rosemary (*Rosmarinus*
284 *officinalis*) leaves. Journal of Supercritical Fluids 55, 971–976.
285 <https://doi.org/10.1016/j.supflu.2010.09.030>.

286 García-Risco, M.R., Vicente, G., Reglero, G., Fornari, T., 2011b. Fractionation of thyme
287 (*Thymus vulgaris* L.) by supercritical fluid extraction and chromatography. The Journal
288 of Supercritical Fluids 55, 949–954. <https://doi.org/10.1016/j.supflu.2010.10.008>.

289 Huang, Z., Shi, X.-H., Jiang, W.-J., 2012. Theoretical models for supercritical fluid extraction.
290 Journal of chromatography. A 1250, 2–26.
291 <https://doi.org/10.1016/j.chroma.2012.04.032>.

292 Huwaldt, J.A., Steinhorst, S., 2014. Plot Digitizer.

293 López-Padilla, A., Ruiz-Rodriguez, A., Reglero, G., Fornari, T., 2017. Supercritical carbon
294 dioxide extraction of *Calendula officinalis*: kinetic modeling and scaling up study.
295 Journal of Supercritical Fluids. In press. <https://doi.org/10.1016/j.supflu.2017.03.033>.

296 López-Padilla, A., Ruiz-Rodriguez, A., Reglero, G., Fornari, T., 2016a. Study of the diffusion
297 coefficient of solute-type extracts in supercritical carbon dioxide: Volatile oils, fatty
298 acids and fixed oils. Journal of Supercritical Fluids 109, 148–156.
299 <https://doi.org/10.1016/j.supflu.2015.11.017>.

300 López-Padilla, A., Ruiz-Rodriguez, A., Restrepo Flórez, C., Rivero Barrios, D., Reglero, G.,

301 Fornari, T., 2016b. *Vaccinium meridionale* Swartz Supercritical CO₂ Extraction: Effect
302 of Process Conditions and Scaling Up. *Materials* 9, 519. Doi:10.3390/ma9070519.

303 Martinez, J., Monteiro, A.R., Rosa, P.T.V., Marques, M.O.M., Meireles, M.A., 2003.
304 Multicomponent model to describe extraction of ginger oleoresin with supercritical
305 carbon dioxide. *Industrial & Engineering Chemistry Research* 42, 1057–1063.
306 Doi:10.1021/ie020694f.

307 Nguyen, K., Barton, P., Spencer, J.S., 1991. Supercritical Carbon Dioxide Extraction of Vanilla.
308 *Journal of Supercritical Fluids* 4, 40–46. [https://doi.org/10.1016/0896-8446\(91\)90029-](https://doi.org/10.1016/0896-8446(91)90029-6)
309 6.

310 NIST, 2017. Thermophysical properties of fluid systems [WWW Document]. National
311 Institute of Standards and Technology. URL <http://webbook.nist.gov/chemistry/fluid/>
312 (accessed 5.16.17).

313 Oliveira, E.L.G., Silvestre, A.J.D., Silva, C.M., 2011. Review of kinetic models for supercritical
314 fluid extraction. *Chemical Engineering Research and Design* 89, 1104–1117.
315 <https://doi.org/10.1016/j.cherd.2010.10.025>.

316 Paula, J.T., Aguiar, A.C., Sousa, I.M.O., Magalhães, P.M., Foglio, M.A., Cabral, F.A., 2016.
317 Scale-up study of supercritical fluid extraction process for *Baccharis dracunculifolia*.
318 *Journal of Supercritical Fluids* 107, 219–225.
319 <https://doi.org/10.1016/j.supflu.2015.09.013>.

320 Povh, N.P., Marques, M.O.M., Meireles, M.A., 2001. Supercritical CO₂ extraction of essential
321 oil and oleoresin from chamomile (*Chamomilla recutita* [L.] Rauschert). *Journal of*
322 *Supercritical Fluids* 21, 245–256. [https://doi.org/10.1016/S0896-8446\(01\)00096-1](https://doi.org/10.1016/S0896-8446(01)00096-1).

323 Prado, J.M., Dalmolin, I., Carareto, N.D.D., Basso, R.C., Meirelles, A.J.A., Vladimir Oliveira, J.,
324 Batista, E. a. C., Meireles, M.A.A., 2012. Supercritical fluid extraction of grape seed:
325 Process scale-up, extract chemical composition and economic evaluation. *Journal of*
326 *Food Engineering* 109, 249–257. <https://doi.org/10.1016/j.jfoodeng.2011.10.007>.

327 Prado, J.M., Prado, G.H.C., Meireles, M.A.A., 2011. Scale-up study of supercritical fluid
328 extraction process for clove and sugarcane residue. *Journal of Supercritical Fluids* 56,
329 231–237. doi: <https://doi.org/10.1016/j.supflu.2010.10.036>.

330 Silva, C.F., Mendes, M.F., Pessoa, F.L.P., Queiroz, E.M., 2008. Supercritical carbon dioxide
331 extraction of macadamia (*Macadamia integrifolia*) nut oil: experiments and modeling.
332 *Brazilian Journal of Chemical Engineering* 25, 175–181.
333 <http://dx.doi.org/10.1590/S0104-66322008000100018>.

334 Silva, C.F., Moura, F.C., Mendes, M.F., Pessoa, F.L.P., 2011. Extraction of citronella
335 (*Cymbopogon nardus*) essential oil using supercritical CO₂: Experimental data and
336 mathematical modeling. *Brazilian Journal of Chemical Engineering* 28, 343–350.
337 <http://dx.doi.org/10.1590/S0104-66322011000200019>.

338 Silva, L.P.S., Martínez, J., 2014. Mathematical modeling of mass transfer in supercritical fluid
339 extraction of oleoresin from red pepper. *Journal of Food Engineering* 133, 30–39.
340 <https://doi.org/10.1016/j.jfoodeng.2014.02.013>.

- 341 Sovova, H., 2017. Broken and intact cell model for supercritical fluid extraction: its origin and
342 limits. The Journal of Supercritical Fluids, In press.
343 <https://doi.org/10.1016/j.supflu.2017.02.014>
- 344 Sovová, H., 1994. Rate of the vegetable oil extraction with supercritical CO₂—I. Modelling of
345 extraction curves. Chemical Engineering Science 49, 409–414.
346 [https://doi.org/10.1016/0009-2509\(94\)87012-8](https://doi.org/10.1016/0009-2509(94)87012-8).
- 347 Tegeler, C., Span, R., Wagner, W., 1999. A New Equation of State for Argon covering the fluid
348 region for temperatures from the melting line to 700 K at pressures up to 1000 MPa.
349 Journal of Physical and Chemical Reference Data 28, 779–850.
350 <http://dx.doi.org/10.1063/1.556037>.
- 351 Villanueva-Bermejo, D., Zahran, F., García-Risco, M.R., Reglero, G., Fornari, T., 2017.
352 Supercritical fluid extraction of Bulgarian *Achillea millefolium*. The Journal of
353 Supercritical Fluids 119, 283–288. <https://doi.org/10.1016/j.supflu.2016.10.005>.
- 354 Yesil-Celiktas, O., Otto, F., Gruener, S., Parlar, H., 2009. Determination of extractability of
355 pine bark using supercritical CO₂ extraction and different solvents: Optimization and
356 prediction. Journal of Agricultural and Food Chemistry 57, 341–347.
357 Doi:10.1021/jf8026414
- 358 Zabet, G.L., Moraes, M.N., Meireles, M.A., 2014a. Influence of the bed geometry on the
359 kinetics of rosemary compounds extraction with supercritical CO₂. Journal of
360 Supercritical Fluids 94, 234–244. <https://doi.org/10.1016/j.supflu.2014.07.020>.
- 361 Zabet, G.L., Moraes, M.N., Petenate, A.J., Meireles, M.A., 2014b. Influence of the bed
362 geometry on the kinetics of the extraction of clove bud oil with supercritical CO₂. The
363 Journal of Supercritical Fluids 93, 56–66.
364 <https://doi.org/10.1016/j.supflu.2013.10.001>.
- 365 Zancan, K.C., Marques, M.O.M., Petenate, A.J., Meireles, M.A., 2002. Extraction of ginger
366 (*Zingiber officinale* roscoe) oleoresin with CO₂ and co-solvents: A study of the
367 antioxidant action of the extracts. Journal of Supercritical Fluids 24, 57–76.
368 [https://doi.org/10.1016/S0896-8446\(02\)00013-X](https://doi.org/10.1016/S0896-8446(02)00013-X).

370 **Table 1.** NOVALINDUS facilities for the SFE of solid materials.

371

Characteristics	Lab Scale 1	Lab Scale 2	Pilot Scale
L: Bed length (m)	0.188	0.388	0.570
D: Bed diameter (m)	0.043	0.07	0.107
Bed volume (m ³)	2.7×10 ⁻⁴	1.35×10 ⁻³	5.19×10 ⁻³
Cross flow area (m ²)	1.45×10 ⁻³	3.53×10 ⁻³	8.99×10 ⁻³
Ratio L/D	4.372	5.716	5.327
Cyclone volume (m ³)	5×10 ⁻⁴	5×10 ⁻⁴	1.57×10 ⁻³
Pump capacity (kg/h)	0.2 - 12	0.2 - 12	2.2 - 147
Pressure work (MPa)	0.1 - 69	0.1 - 69	0.1 - 44
Temperature work (°C)	5 - 40	5 - 40	5 - 40
Demister (m ³)	1.71×10 ⁻³	1.71×10 ⁻³	1.5×10 ⁻²
Filter (m ³)	No	No	5×10 ⁻²
Storage tank (m ³)	1.5×10 ⁻²	1.5×10 ⁻²	8.8×10 ⁻²
Recycler system CO ₂	Yes	Yes	Yes
Automated BPR	Yes	Yes	Yes
Flowmeter	Yes	Yes	No
PLC control	Yes	Yes	Yes

372

373

374

375

376

377

378

379

Table 2. SFE data of different OECs obtained in NOVALINDUS Platform.

	Raw Material	Scientific name	D (m)	L (m)	F (kg)	$d_p \times 10^4$ (m)	ρ_B (kg/m ³)	ε	$Q \times 10^3$ (kg/s)	T (K)	P (bar)	ρ_{CO_2} (kg/m ³)	$\mu_{CO_2} \times 10^5$ (kg/m·s)	$D_{E-CO_2} \times 10^8$ (m ² /s)	S_c	Ref.
1	Origanum	<i>Origanum vulgare</i>	0.076	0.416	0.60	5.0	1020	0.69	1.00	313	300	909.9	9.38	1.18	8.725	(Fornari et al., 2012)
2	Sage	<i>Salvia officinalis</i>	0.076	0.416	0.60	5.0	1050	0.70	1.00	313	300	909.9	9.38	1.18	8.725	(Fornari et al., 2012)
3	Thyme	<i>Thymus zygis</i>	0.076	0.416	0.60	10.0	1580	0.80	1.00	313	300	909.9	9.38	1.18	8.725	(Fornari et al., 2012)
4	Rosemary	<i>Rosmarinus officinalis</i>	0.076	0.416	0.60	10.0	1046	0.70	1.00	313	300	909.9	9.38	1.18	8.725	(Fornari et al., 2012)
5	Rosemary	<i>Rosmarinus officinalis</i>	0.076	0.416	0.60	10.0	1046	0.70	1.00	314	300	909.9	9.38	1.18	8.713	(García-Risco et al., 2011a)
6	Rosemary	<i>Rosmarinus officinalis</i>	0.076	0.416	0.60	10.0	1046	0.70	1.00	315	300	909.9	9.38	1.19	8.701	(García-Risco et al., 2011a)
7	Thyme	<i>Thymus vulgaris</i> L.	0.076	0.416	0.55	4.0	1580	0.82	0.67	313	150	841.0	6.36	1.14	6.621	(García-Risco et al., 2011b)
8	Yarrow	<i>Achillea millefolium</i>	0.067	0.383	0.40	5.0	1015	0.71	1.20	313	140	763.0	6.50	1.49	5.705	(Villanueva-Bermejo et al., 2017)
9	Calendula	<i>Calendula officinalis</i>	0.043	0.188	0.09	5.0	1409	0.76	0.25	313	140	763.0	6.50	1.49	5.702	(López-Padilla et al., 2017)
10	Calendula	<i>Calendula officinalis</i>	0.043	0.188	0.09	5.0	1409	0.76	0.50	313	140	763.0	6.50	1.49	5.702	(López-Padilla et al., 2017)
11	Calendula	<i>Calendula officinalis</i>	0.043	0.188	0.09	5.0	1409	0.76	0.75	313	140	763.0	6.50	1.49	5.702	(López-Padilla et al., 2017)
12	Calendula	<i>Calendula officinalis</i>	0.043	0.188	0.09	5.0	1409	0.76	0.50	313	240	872.5	8.51	1.25	7.829	(López-Padilla et al., 2017)
13	Calendula	<i>Calendula officinalis</i>	0.043	0.188	0.09	5.0	1409	0.76	0.50	313	340	930.2	9.91	1.15	9.238	(López-Padilla et al., 2017)
14	Calendula	<i>Calendula officinalis</i>	0.067	0.383	0.45	5.0	1409	0.76	0.60	313	140	763.0	6.50	1.49	5.702	(López-Padilla et al., 2017)
15	Calendula	<i>Calendula officinalis</i>	0.067	0.383	0.45	5.0	1409	0.76	1.23	313	140	763.0	6.50	1.49	5.702	(López-Padilla et al., 2017)
16	Calendula	<i>Calendula officinalis</i>	0.107	0.570	1.71	5.0	1409	0.76	1.54	313	140	763.0	6.50	1.49	5.702	(López-Padilla et al., 2017)
17	Calendula	<i>Calendula officinalis</i>	0.107	0.570	1.71	5.0	1409	0.76	4.70	313	140	763.0	6.50	1.49	5.702	(López-Padilla et al., 2017)
18	Mortiño	<i>Vaccinium merdionale</i>	0.043	0.188	0.16	2.5	1440	0.59	0.53	313	300	909.9	9.38	1.18	8.724	(López-Padilla et al., 2016b)
19	Mortiño	<i>Vaccinium merdionale</i>	0.067	0.383	0.80	2.5	1440	0.59	2.63	313	300	909.9	9.38	1.18	8.724	(López-Padilla et al., 2016b)

383 **Table 3.** SFE data of OECs obtained from the literature.

	Raw Material	Scientific name	D (m)	L (m)	F (kg)	$d_p \times 10^4$ (m)	ρ_B (kg/m ³)	ε	$Q \times 10^3$ (kg/s)	T (K)	P (bar)	ρ_{CO_2} (kg/m ³)	$\mu_{CO_2} \times 10^5$ (kg/m·s)	$D_{E-CO_2} \times 10^8$ (m ² /s)	S_c	Ref.
1	Red pepper	<i>Capsicum frutescens</i>	0.030	0.075	0.024	9.3	1320	0.66	0.402	313	150	780.2	6.77	0.93	9.289	(Silva and Martínez, 2014)
2	Red pepper	<i>Capsicum frutescens</i>	0.030	0.129	0.042	9.3	1320	0.66	0.402	313	150	780.2	6.77	0.93	9.289	(Silva and Martínez, 2014)
3	Red pepper	<i>Capsicum frutescens</i>	0.054	0.125	0.128	9.3	1320	0.66	0.402	313	150	780.2	6.77	0.93	9.289	(Silva and Martínez, 2014)
4	Red pepper	<i>Capsicum frutescens</i>	0.054	0.125	0.125	4.3	1320	0.67	0.402	313	150	780.2	6.77	0.93	9.289	(Silva and Martínez, 2014)
5	Red pepper	<i>Capsicum frutescens</i>	0.054	0.125	0.125	4.3	1320	0.67	0.285	313	150	780.2	6.77	0.93	9.289	(Silva and Martínez, 2014)
6	Red pepper	<i>Capsicum frutescens</i>	0.054	0.125	0.125	4.3	1320	0.67	0.170	313	150	780.2	6.77	0.93	9.289	(Silva and Martínez, 2014)
7	Red pepper	<i>Capsicum frutescens</i>	0.030	0.129	0.040	4.3	1320	0.67	0.170	313	150	780.2	6.77	0.93	9.289	(Silva and Martínez, 2014)
8	Red pepper	<i>Capsicum frutescens</i>	0.030	0.129	0.042	9.3	1320	0.66	0.170	313	150	780.2	6.77	0.93	9.289	(Silva and Martínez, 2014)
9	Red pepper	<i>Capsicum frutescens</i>	0.030	0.129	0.041	14.1	1320	0.67	0.170	313	150	780.2	6.77	0.93	9.289	(Silva and Martínez, 2014)
10	Red pepper	<i>Capsicum frutescens</i>	0.030	0.075	0.023	4.3	1320	0.68	0.285	313	150	780.2	6.77	0.93	9.289	(Silva and Martínez, 2014)
11	Red pepper	<i>Capsicum frutescens</i>	0.030	0.075	0.024	9.3	1320	0.66	0.285	313	150	780.2	6.77	0.93	9.289	(Silva and Martínez, 2014)
12	Red pepper	<i>Capsicum frutescens</i>	0.030	0.075	0.024	14.1	1320	0.67	0.285	313	150	780.2	6.77	0.93	9.289	(Silva and Martínez, 2014)
13	Red pepper	<i>Capsicum frutescens</i>	0.030	0.129	0.041	14.1	1320	0.67	0.285	313	150	780.2	6.77	0.93	9.289	(Silva and Martínez, 2014)
14	Red pepper	<i>Capsicum frutescens</i>	0.030	0.075	0.023	4.3	1320	0.68	0.402	313	150	780.2	6.77	0.93	9.289	(Silva and Martínez, 2014)
15	Red pepper	<i>Capsicum frutescens</i>	0.030	0.129	0.040	4.3	1320	0.67	0.402	313	150	780.2	6.77	0.93	9.289	(Silva and Martínez, 2014)
16	Red pepper	<i>Capsicum frutescens</i>	0.030	0.129	0.041	14.1	1320	0.67	0.402	313	150	780.2	6.77	0.93	9.289	(Silva and Martínez, 2014)
17	chamomile	<i>Chamomilla recutita</i>	0.040	0.166	0.075	3.0	1346	0.72	0.067	303	100	771.5	6.61	1.45	5.897	(Povh et al., 2001)
18	chamomile	<i>Chamomilla recutita</i>	0.040	0.166	0.075	3.0	1346	0.72	0.067	303	120	808.9	7.24	1.36	6.572	(Povh et al., 2001)
19	chamomile	<i>Chamomilla recutita</i>	0.040	0.166	0.075	3.0	1346	0.72	0.067	303	160	857.1	8.17	1.26	7.579	(Povh et al., 2001)
20	chamomile	<i>Chamomilla recutita</i>	0.040	0.166	0.075	3.0	1346	0.72	0.067	303	200	890.5	8.91	1.20	8.364	(Povh et al., 2001)
21	chamomile	<i>Chamomilla recutita</i>	0.040	0.166	0.075	3.0	1346	0.72	0.067	313	100	628.7	4.02	1.80	3.563	(Povh et al., 2001)
22	chamomile	<i>Chamomilla recutita</i>	0.040	0.166	0.075	3.0	1346	0.72	0.033	313	120	717.8	5.85	1.62	5.046	(Povh et al., 2001)

384 **Table 3.** SFE data of OECs obtained from the literature (Continuation).

	Raw Material	Scientific name	D (m)	L (m)	F (kg)	$d_p \times 10^4$ (m)	ρ_B (kg/m ³)	ε	$Q \times 10^3$ (kg/s)	T (K)	P (bar)	ρ_{CO_2} (kg/m ³)	$\mu_{CO_2} \times 10^5$ (kg/m·s)	$D_{E-CO_2} \times 10^8$ (m ² /s)	S_c	Ref.
23	chamomile	<i>Chamomilla recutita</i>	0.040	0.166	0.075	3.0	1346	0.72	0.067	313	120	717.8	5.12	1.53	4.651	(Povh et al., 2001)
24	chamomile	<i>Chamomilla recutita</i>	0.040	0.166	0.075	3.0	1346	0.72	0.067	313	160	792.2	6.69	1.39	6.082	(Povh et al., 2001)
25	chamomile	<i>Chamomilla recutita</i>	0.040	0.166	0.075	3.0	1346	0.72	0.033	313	160	794.9	7.02	1.41	6.245	(Povh et al., 2001)
26	chamomile	<i>Chamomilla recutita</i>	0.040	0.166	0.075	3.0	1346	0.72	0.067	313	200	839.9	7.79	1.31	7.103	(Povh et al., 2001)
27	Ginger	<i>Zingiber officinale</i>	0.028	0.375	0.080	10.2	1300	0.74	0.056	313	250	881.0	8.82	1.24	8.049	(Martinez et al., 2003)
28	Ginger	<i>Zingiber officinale</i>	0.028	0.375	0.080	10.2	1300	0.74	0.056	303	150	847.0	7.86	1.27	7.326	(Martinez et al., 2003)
29	Ginger	<i>Zingiber officinale</i>	0.028	0.375	0.080	10.2	1300	0.74	0.056	313	200	841.0	7.79	1.30	7.119	(Martinez et al., 2003)
30	Ginger	<i>Zingiber officinale</i>	0.028	0.375	0.080	10.2	1300	0.74	0.056	313	150	841.0	6.36	1.14	6.621	(Martinez et al., 2003)
31	Ginger	<i>Zingiber officinale</i>	0.028	0.387	0.008	3.9	1524	0.97	0.059	298	200	914.2	9.97	1.20	9.056	(Zancan et al., 2002)
32	Ginger	<i>Zingiber officinale</i>	0.028	0.387	0.008	3.9	1524	0.97	0.060	298	250	943.5	10.3	1.11	9.793	(Zancan et al., 2002)
33	Ginger	<i>Zingiber officinale</i>	0.028	0.387	0.008	3.9	1524	0.97	0.059	308	200	866.2	8.46	1.26	7.757	(Zancan et al., 2002)
34	Ginger	<i>Zingiber officinale</i>	0.028	0.387	0.008	3.9	1524	0.97	0.059	308	250	901.8	9.17	1.18	8.582	(Zancan et al., 2002)
35	Rosemary	<i>Rosmarinus officinalis</i>	0.034	0.095	0.031	6.6	1046	0.66	0.083	313	300	909.9	9.91	1.24	8.78	(Carvalho et al., 2005)
36	Rosemary	<i>Rosmarinus officinalis</i>	0.034	0.190	0.061	6.6	1046	0.66	0.083	313	300	909.9	9.91	1.24	8.78	(Carvalho et al., 2005)
37	Rosemary	<i>Rosmarinus officinalis</i>	0.034	0.285	0.092	6.6	1046	0.66	0.083	313	300	909.9	9.91	1.24	8.78	(Carvalho et al., 2005)
38	Rosemary	<i>Rosmarinus officinalis</i>	0.034	0.037	0.031	6.6	1046	0.66	0.052	313	300	909.9	9.91	1.24	8.78	(Carvalho et al., 2005)
39	Rosemary	<i>Rosmarinus officinalis</i>	0.034	0.073	0.061	6.6	1046	0.66	0.083	313	300	909.9	9.91	1.24	8.78	(Carvalho et al., 2005)

385

386

387

Table 4. Barton kinetic constants of OECs obtained in NOVALINDUS Platform.

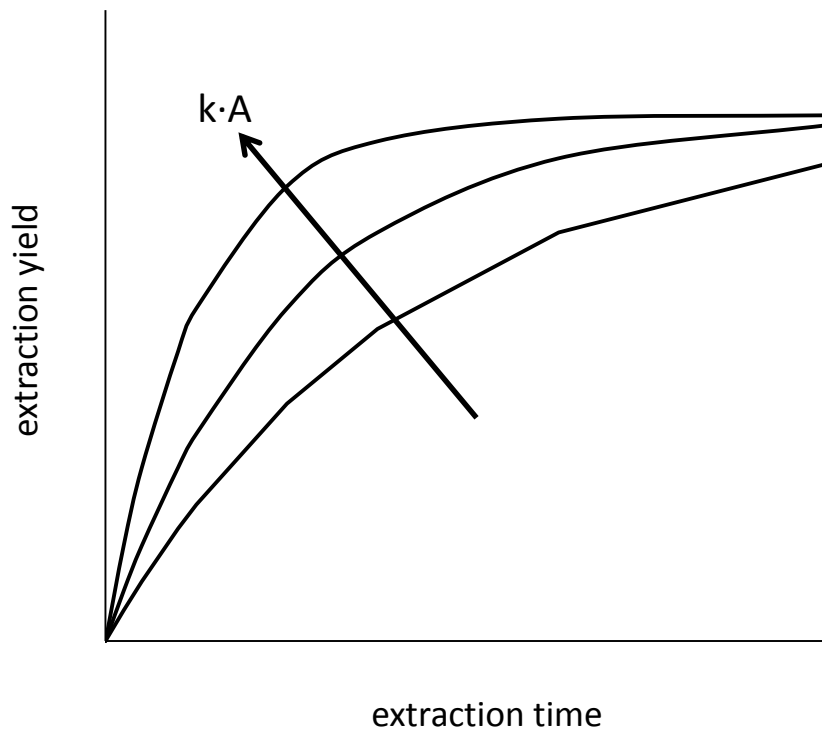
	Raw Material	Scientific name	k (min ⁻¹)	Y _∞	R ²	Ref.
1	Origanum	<i>O. vulgare</i>	0.0182	0.048	0.980	(Fornari et al., 2012)
2	Sage	<i>S. officinalis</i>	0.0177	0.047	0.995	(Fornari et al., 2012)
3	Thyme	<i>T. zygis</i>	0.0099	0.033	0.995	(Fornari et al., 2012)
4	Rosemary	<i>R. officinalis</i>	0.0094	0.038	0.969	(Fornari et al., 2012)
5	Rosemary	<i>R. officinalis</i>	0.0078	0.049	0.959	(García-Risco et al., 2011a)
6	Rosemary	<i>R. officinalis</i>	0.0085	0.043	0.988	(García-Risco et al., 2011a)
7	Thyme	<i>T. vulgaris</i> L.	0.0132	0.032	0.999	(García-Risco et al., 2011b)
8	Yarrow	<i>A. millefolium</i>	0.0151	0.030	0.963	(Villanueva-Bermejo et al., 2017)
9	Calendula	<i>C. officinalis</i>	0.0091	0.050	0.984	(López-Padilla et al., 2017)
10	Calendula	<i>C. officinalis</i>	0.0112	0.059	0.974	(López-Padilla et al., 2017)
11	Calendula	<i>C. officinalis</i>	0.0127	0.063	0.963	(López-Padilla et al., 2017)
12	Calendula	<i>C. officinalis</i>	0.0143	0.064	0.985	(López-Padilla et al., 2017)
13	Calendula	<i>C. officinalis</i>	0.0175	0.065	0.969	(López-Padilla et al., 2017)
14	Calendula	<i>C. officinalis</i>	0.0081	0.035	0.986	(López-Padilla et al., 2017)
15	Calendula	<i>C. officinalis</i>	0.0095	0.045	0.988	(López-Padilla et al., 2017)
16	Calendula	<i>C. officinalis</i>	0.0082	0.053	0.973	(López-Padilla et al., 2017)
17	Calendula	<i>C. officinalis</i>	0.0113	0.078	0.998	(López-Padilla et al., 2017)
18	Mortiño	<i>V. merdionale</i>	0.0429	0.032	0.925	(López-Padilla et al., 2016b)
19	Mortiño	<i>V. merdionale</i>	0.0511	0.032	0.909	(López-Padilla et al., 2016b)

Table 5. Barton kinetic constants of OECs obtained from the literature.

	Raw Material	Scientific name	k (min ⁻¹)	Y _∞	R ²	Ref.
1	Red pepper	<i>C. frutescens</i>	0.0270	0.5300	0.917	(Silva and Martínez, 2014)
2	Red pepper	<i>C. frutescens</i>	0.0216	0.5947	0.953	(Silva and Martínez, 2014)
3	Red pepper	<i>C. frutescens</i>	0.0118	0.0553	0.996	(Silva and Martínez, 2014)
4	Red pepper	<i>C. frutescens</i>	0.0141	0.0912	0.951	(Silva and Martínez, 2014)
5	Red pepper	<i>C. frutescens</i>	0.0105	0.0778	0.953	(Silva and Martínez, 2014)
6	Red pepper	<i>C. frutescens</i>	0.0076	0.0475	0.959	(Silva and Martínez, 2014)
7	Red pepper	<i>C. frutescens</i>	0.0124	0.0860	0.989	(Silva and Martínez, 2014)
8	Red pepper	<i>C. frutescens</i>	0.0153	0.0535	0.993	(Silva and Martínez, 2014)
9	Red pepper	<i>C. frutescens</i>	0.0122	0.0409	0.996	(Silva and Martínez, 2014)
10	Red pepper	<i>C. frutescens</i>	0.0295	0.0875	0.980	(Silva and Martínez, 2014)
11	Red pepper	<i>C. frutescens</i>	0.0263	0.0568	0.981	(Silva and Martínez, 2014)
12	Red pepper	<i>C. frutescens</i>	0.0235	0.0423	0.966	(Silva and Martínez, 2014)
13	Red pepper	<i>C. frutescens</i>	0.0148	0.0460	0.971	(Silva and Martínez, 2014)
14	Red pepper	<i>C. frutescens</i>	0.0416	0.1046	0.950	(Silva and Martínez, 2014)
15	Red pepper	<i>C. frutescens</i>	0.0244	0.0958	0.968	(Silva and Martínez, 2014)
16	Red pepper	<i>C. frutescens</i>	0.0220	0.0510	0.982	(Silva and Martínez, 2014)
17	chamomile	<i>C. recutita</i>	0.0053	0.0339	0.996	(Povh et al., 2001)
18	chamomile	<i>C. recutita</i>	0.0049	0.0320	0.994	(Povh et al., 2001)
19	chamomile	<i>C. recutita</i>	0.0058	0.0390	0.995	(Povh et al., 2001)
20	chamomile	<i>C. recutita</i>	0.0075	0.0391	0.994	(Povh et al., 2001)
21	chamomile	<i>C. recutita</i>	0.0046	0.0219	0.994	(Povh et al., 2001)
22	chamomile	<i>C. recutita</i>	0.0030	0.0528	0.998	(Povh et al., 2001)
23	chamomile	<i>C. recutita</i>	0.0063	0.0324	0.998	(Povh et al., 2001)
24	chamomile	<i>C. recutita</i>	0.0052	0.0376	0.984	(Povh et al., 2001)
25	chamomile	<i>C. recutita</i>	0.0039	0.0539	0.996	(Povh et al., 2001)
26	chamomile	<i>C. recutita</i>	0.0079	0.0440	0.985	(Povh et al., 2001)
27	Ginger	<i>Z. officinale</i>	0.0037	0.6465	0.985	(Martinez et al., 2003)
28	Ginger	<i>Z. officinale</i>	0.0025	0.0450	0.958	(Martinez et al., 2003)
29	Ginger	<i>Z. officinale</i>	0.0038	0.0494	0.964	(Martinez et al., 2003)
30	Ginger	<i>Z. officinale</i>	0.0033	0.0421	0.978	(Martinez et al., 2003)
31	Ginger	<i>Z. officinale</i>	0.0084	0.0342	0.994	(Zancan et al., 2002)
32	Ginger	<i>Z. officinale</i>	0.0078	0.0375	0.982	(Zancan et al., 2002)
33	Ginger	<i>Z. officinale</i>	0.0070	0.0251	0.992	(Zancan et al., 2002)
34	Ginger	<i>Z. officinale</i>	0.0086	0.0208	0.980	(Zancan et al., 2002)
35	Rosemary	<i>R. officinalis</i>	0.0102	0.0458	0.997	(Carvalho et al., 2005)
36	Rosemary	<i>R. officinalis</i>	0.0107	0.0372	0.993	(Carvalho et al., 2005)
37	Rosemary	<i>R. officinalis</i>	0.0094	0.0363	0.980	(Carvalho et al., 2005)
38	Rosemary	<i>R. officinalis</i>	0.0108	0.0429	0.989	(Carvalho et al., 2005)
39	Rosemary	<i>R. officinalis</i>	0.0112	0.0405	0.967	(Carvalho et al., 2005)

393

394

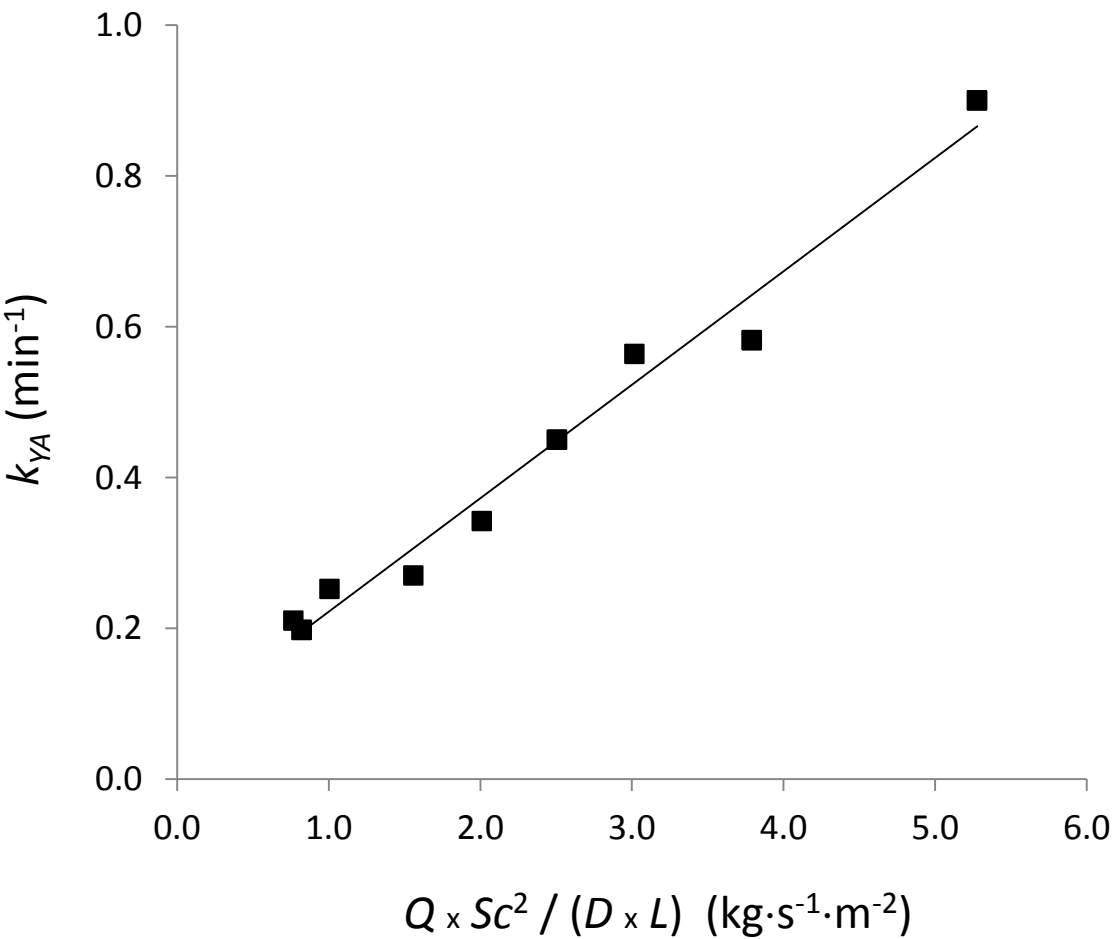


395

396 **Figure 1.** General shape of the Overall Extraction Curve (OEC): effect of mass transfer
397 coefficient and interfacial area.

398

399

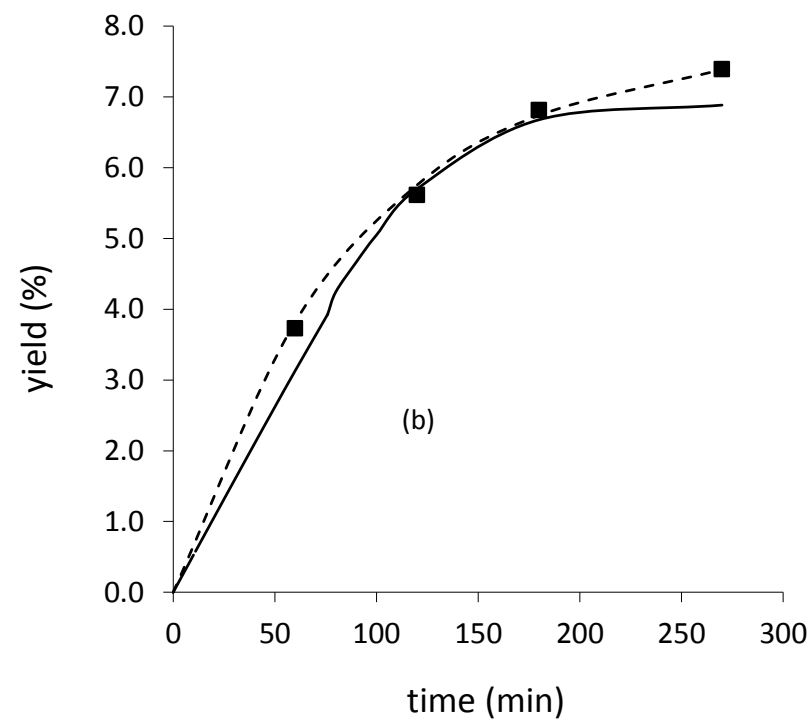
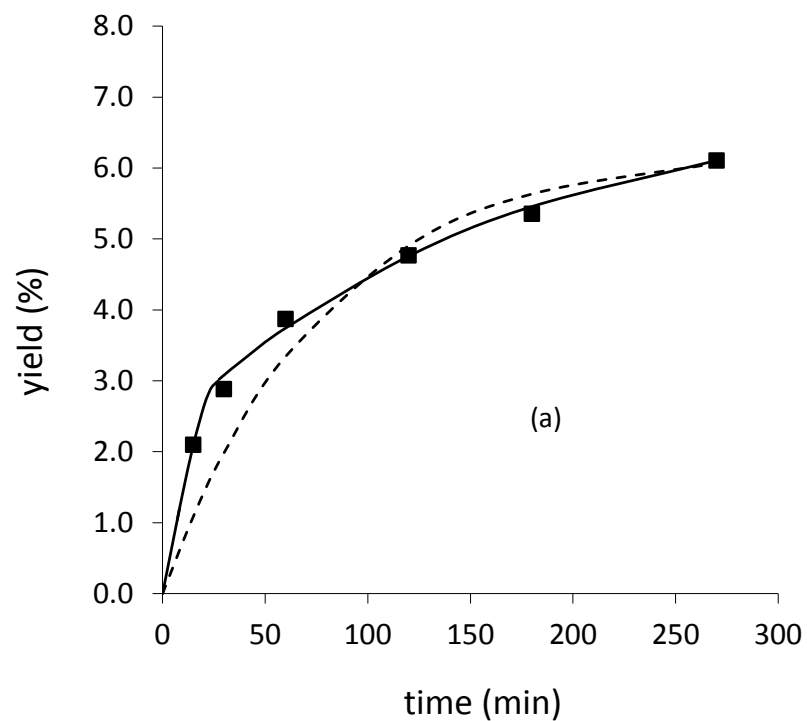


400

401 **Figure 2.** Correlation between BIC model mass transfer coefficient in the supercritical fluid
402 phase (k_{YA}) and the CO₂ flow rate (Q) of nine OECs corresponding to calendula SFE (López-
403 Padilla et al., 2017) at constant bed porosity and constant mean particle diameter ($R^2 =$
404 0.9767).

405

406



40

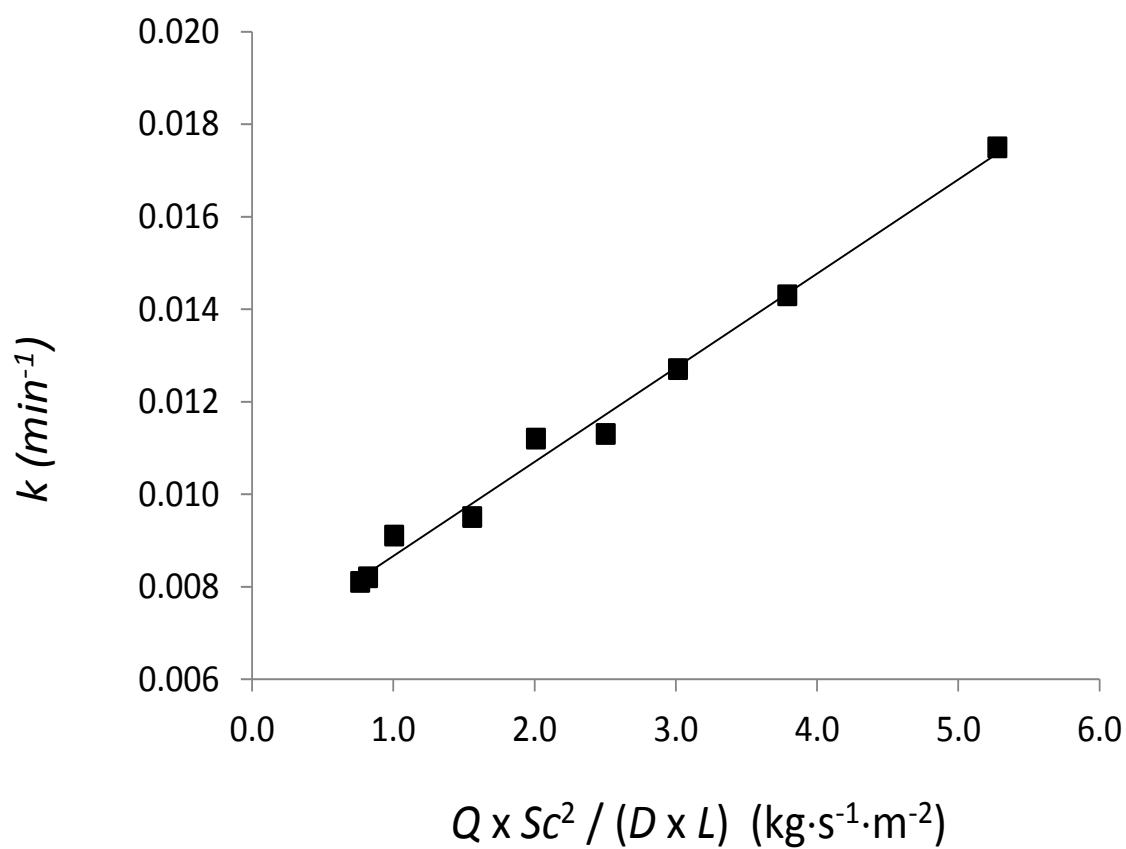
408 **Figure 3.** Comparison between BIC and Barton models in the fitting of calendula OECs 11 and 17 of Table 2. Solid line: BIC model; dashed line:
409 Barton model.

410

411

412

413



414

415

416 **Figure 4.** Correlation between Barton model kinetic constant (k) and the CO₂ flow rate (Q)
 417 of nine OECs corresponding to calendula SFE at constant bed porosity and constant mean
 418 particle diameter ($R^2 = 0.9906$).

419

420

421

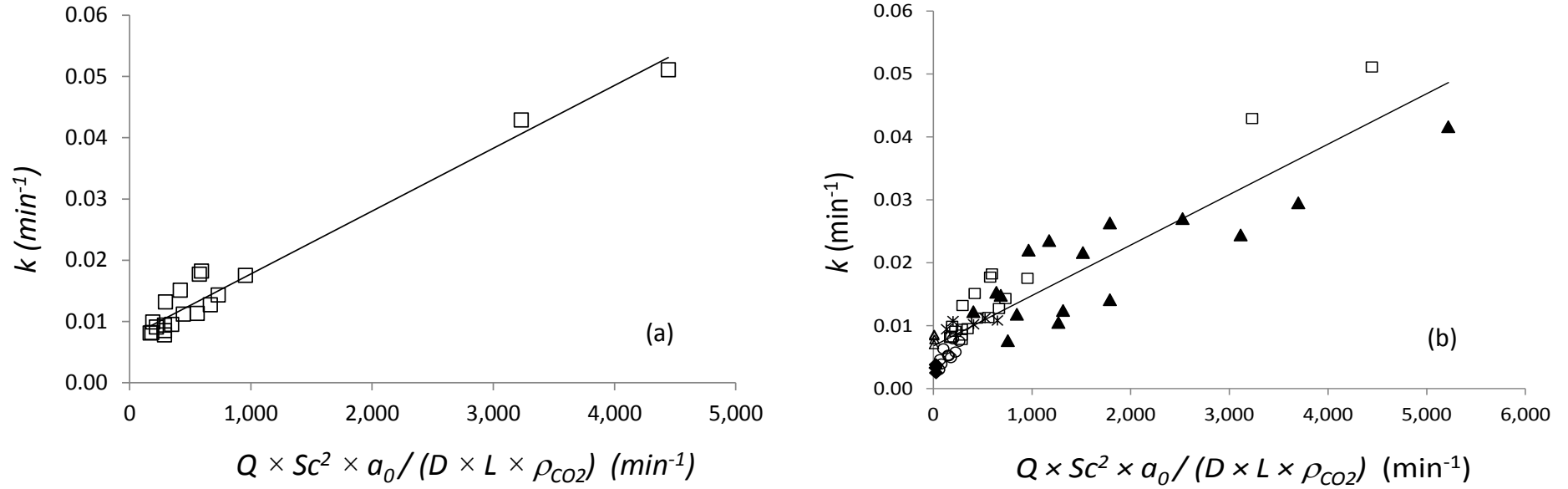
422

423

424

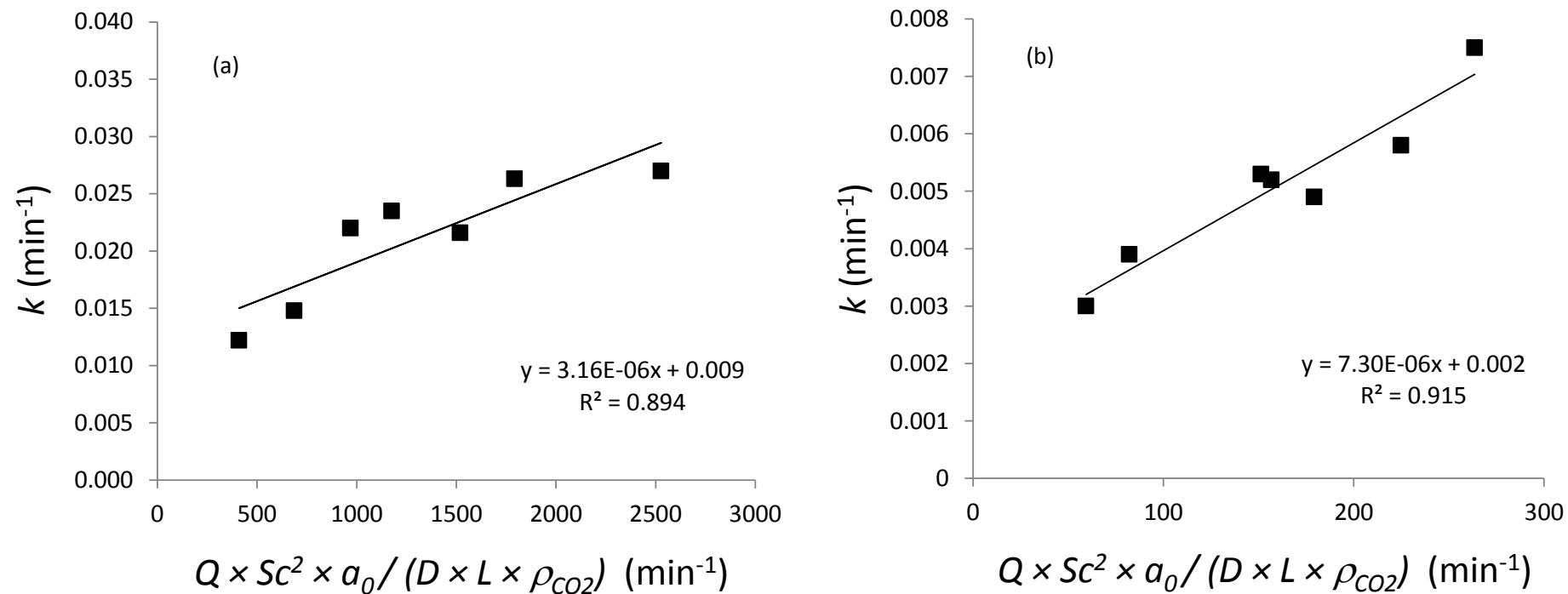
425

426



429 **Figure 5.** Correlation between Barton model kinetic constant (k) and the CO₂ flow rate (Q) of the OECs studied in this work: (a) Table 2
 430 (NOVALINDUS Platform) $R^2 = 0.9624$; (b) Tables 2 and 3, $R^2 = 0.8328$. (\square) NOVALINDUS (Fornari et al., 2012; García-Risco et al., 2011a; López-
 431 Padilla et al., 2017; López-Padilla et al., 2016b; Villanueva-Bermejo et al., 2017); (\blacktriangle) Silva and Martínez, 2014; (\circ) Povh et al., 2001; (\triangle)
 432 Martinez et al., 2003; (\blacklozenge) Zancan et al., 2002; ($*$) Carvalho et al., 2005.

435



436

437

438 **Figure 6.** Correlation between Barton model kinetic constant (k) and the CO₂ flow rate (Q) of the OECs with (a) high Reynold numbers (7.37 to

439 17.43) and (b) small Reynold numbers (0.16-0.34).

440

441

442

443